Magnon photon coupling for magnetization antiparallel to the magnetic field

Y. Xiao,[1] X. H. Yan,[2] L. H. Bai,[3] H. Guo,[4] C. M. Hu,[5] and K. Xia[6]

[1]*College of Science, Nanjing University of Aeronautics and Astronautics, Nanjing 210016, China*
[2]*School of Material Science and Engineering, Jiangsu University, Zhenjiang 212013, China*
[3]*School of Physics, Shandong University, 27 Shandanan Road, Jinan 250100, China*
[4]*Department of Physics, McGill University, Montreal, Quebec, Canada H3A 2T8*
[5]*Department of Physics and Astronomy, University of Manitoba, Winnipeg, Canada R3T 2N2*
[6]*Shenzhen Institute for Quantum Science and Engineering and Department of Physics, Southern University of Science and Technology, Shenzhen 518055, China*

(Received 1 November 2019; revised 10 March 2021; accepted 12 March 2021; published 23 March 2021)

Current studies of cavity magnon polaritons are focused on ferromagnetic magnons for which the frequency increases with a static magnetic field. In this paper, we propose a ferromagnetic system with magnon frequency decreasing with a static magnetic field. It is achieved by antiparallel alignment between the magnetization and static magnetic field. The magnetization precession is stabilized by a large anisotropic field along the direction of magnetization. The analysis of the Polder tensor shows that the magnon modes in parallel and antiparallel alignments are analogous to those in an antiferromagnet. The strong coupling between a magnon and photon for antiparallel alignment results in an anticrossing gap in the transmission spectrum. Based on the Tavis-Cummings Hamiltonian and Bloch sphere representation, we show that the photon absorption decreases (increases) the spin angular momentum in antiparallel (parallel) alignment. The coupled Hamiltonians of harmonic oscillators are derived and have the same form for both parallel and antiparallel cases. The method developed and results presented are expected to be helpful to realize low-frequency magnon photon coupling that is similar to those in an antiferromagnet.

DOI: 10.1103/PhysRevB.103.104432

I. INTRODUCTION

A cavity magnon polariton [1–8], i.e., a hybrid of a magnon and cavity photon, provides considerable insights into the light-matter interaction and has potential applications in quantum information processing. A number of theories and experiments show that strong coupling between a magnon and cavity photon manifests itself in the anticrossing gap of microwave transmission [9–18] and spin current spectra [19–22]. The strong coupling and the long coherence time of a spin and magnon make the cavity magnon polariton an ideal candidate for the design of spintronic [23,24] and quantum devices [25–27].

Intrinsically, the anticrossing gap represents the repulsive interaction between magnon and photon modes and thus sometimes is called level repulsion [28,29]. Currently, it has been revealed that the level repulsion describes coherent coupling between a magnon and photon with a relative phase of 0 or π [30,31]. In a mathematical form, the coupled mode is written as $\psi_\pm = c_+ h \pm c_- m$ with photon field h, magnetization m, and constants $c_\pm$. In the language of chemistry, the two levels of coupled modes can be thought of as the bonding and antibonding states of a hydrogen molecule [32]. Since the eigenstate is both magnonlike and photonlike, the system energy is distributed on both modes. When viewing the temporal dynamics of the level repulsion, one can find that the energy is exchanged between a magnon and photon. This is reminiscent of Rabi oscillation, which has been observed in recent experimental measurements and predicted in some theoretical works [33,34].

Currently, most studies of cavity magnon polaritons are focused on a ferromagnetic magnon [1–22]. Only some works have studied the coupling between a photon and antiferromagnetic magnon [35–40]. Especially for conventional antiferromagnets, e.g., Cr_2O_3, MnF_2, etc., strong coupling has yet to be reported. The main obstacles are the fabrication of a high-frequency (THz) cavity and the low-damping material. Despite these difficulties, antiferromagnetic magnon photon coupling holds much promise for physics understanding and device applications. In contrast to a ferromagnet, an antiferromagnet is composed of two-sublattice magnetization with two magnon modes, which adds extra tunability into the magnon photon coupling. Second, an antiferromagnet does not display macroscopic magnetization and a stray field. Third, antiferromagnetic spintronics is an emergent field [41] so that the strong coupling between a photon and antiferromagnetic magnon may find potential applications in it.

In this paper, we propose an alternative method to realize magnon photon coupling that is similar to that in an antiferromagnet. As is known, the frequency of one magnon mode in an antiferromagnet increases with a static magnetic field while another one decreases. The former is similar to a ferromagnetic magnon, but the latter one is not easy to find in a ferromagnet. Here, we propose an antiparallel alignment between the magnetization and static magnetic field, which is stabilized by an anisotropic field in the direction of magnetization.

 ©2021 American Physical Society

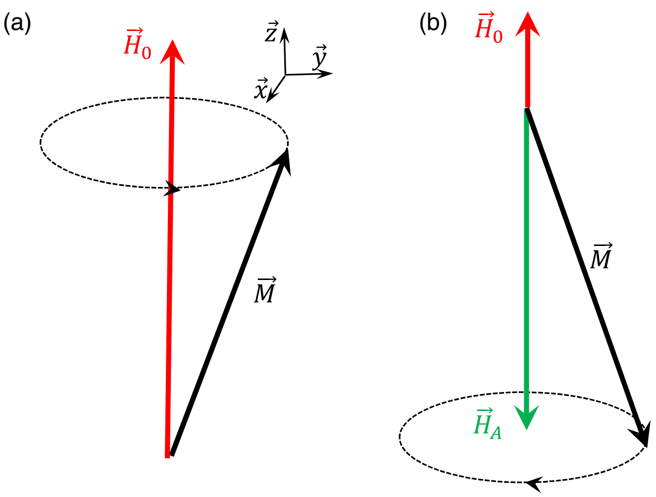

FIG. 1. Magnetization precession in (a) parallel and (b) antiparallel alignment between $\vec{M}$ and $\vec{H}_0$. In (b), a large anisotropic field ($H_A > H_0$) is applied to stabilize the magnetization.

By analysis of the Polder tensor, we find that the magnon mode in such an antiparallel alignment is analogous to the above-mentioned antiferromagnetic magnon. The advantage of this alignment is that the resonance frequency is within the range of microwave frequency.

The remainder of the paper is organized as follows. First, we introduce the model of antiparallel alignment between magnetization and static magnetic field. The Polder susceptibility tensor is analyzed for three cases. With a realistic model of cavity and material parameters, we calculate the transmission coefficient for a yttrium iron garnet (YIG)-embedded microwave cavity with antiparallel alignment. Second, we employ the Tavis-Cummings Hamiltonian, together with the Bloch sphere method, to analyze the behavior of magnon photon coupling in parallel and antiparallel alignments. Finally, the findings are concluded in the summary.

II. POLDER SUSCEPTIBILITY TENSOR

We start by analyzing the Polder susceptibility tensor for three cases. (i) The first is the parallel alignment between magnetization $\vec{M}$ and static magnetic field $\vec{H}_0$ in a ferromagnet. (ii) The second is the antiparallel alignment between $\vec{M}$ and $\vec{H}_0$, which is the focus of this work. In order stabilize the magnetization, we consider a large anisotropic field $\vec{H}_A$ along the direction of $\vec{M}$ with $H_A > H_0$. Cases (i) and (ii) are shown in Figs. 1(a) and 1(b). (iii) For comparison, we also consider an antiferromagnet in which each sublattice magnetization is exerted by a static magnetic field, anisotropic field $\vec{H}_A^a$, and exchange field $\vec{H}_E^a$.

The tensor describes the relation between dynamic magnetization $\vec{m}$ and dynamic field $\vec{h}$. It can be calculated based on the Landau-Lifshitz-Gilbert (LLG) equation [42]

$$\frac{d\vec{m}}{dt} = -\gamma\vec{m} \times \left(\vec{H}_{\text{eff}} + \vec{h}\right) + \alpha\vec{m} \times \frac{d\vec{m}}{dt}, \tag{1}$$

where α is the Gilbert damping rate and γ is the effective gyromagnetic ratio. Under the small-angle precession approximation, the dynamic magnetization in Fourier space ($\sim e^{-i\omega t}$) takes the form of [42]

$$\begin{pmatrix} m_x \\ m_y \end{pmatrix} = \chi \begin{pmatrix} h_x \\ h_y \end{pmatrix}, \tag{2}$$

where χ is the Polder susceptibility tensor.

In case (i), the effective field is $\vec{H}_{\text{eff}} = H_0\vec{z}$. The tensor takes the form of

$$\chi^{(i)} = \gamma M_0 \begin{pmatrix} \frac{(\gamma H_0 - i\alpha\omega)}{(\gamma H_0 - i\alpha\omega)^2 - \omega^2} & -i\frac{\omega}{(\gamma H_0 - i\alpha\omega)^2 - \omega^2} \\ i\frac{\omega}{(\gamma H_0 - i\alpha\omega)^2 - \omega^2} & \frac{(\gamma H_0 - i\alpha\omega)}{(\gamma H_0 - i\alpha\omega)^2 - \omega^2} \end{pmatrix}, \tag{3}$$

where M_0 is the saturation magnetization.

In case (ii), schematically shown in Fig. 1(b), the effective field is $\vec{H}_{\text{eff}} = (H_0 - H_A)\vec{z}$ and aligns along the $-\vec{z}$ direction. The tensor takes the form of

$$\chi^{(ii)} = \gamma M_0 \begin{pmatrix} \frac{(\gamma H_A - \gamma H_0 - i\alpha\omega)}{(\gamma H_A - \gamma H_0 - i\alpha\omega)^2 - \omega^2} & i\frac{\omega}{(\gamma H_A - \gamma H_0 - i\alpha\omega)^2 - \omega^2} \\ -i\frac{\omega}{(\gamma H_A - \gamma H_0 - i\alpha\omega)^2 - \omega^2} & \frac{(\gamma H_A - \gamma H_0 - i\alpha\omega)}{(\gamma H_A - \gamma H_0 - i\alpha\omega)^2 - \omega^2} \end{pmatrix}. \tag{4}$$

In case (iii), an antiferromagnet consists of two sublattice magnetizations, i.e., A and B. The effective field of each sublattice magnetization is $\vec{H}_{\text{eff}}^{(A,B)} = H_0\vec{z} \pm H_A^a\vec{z} - \vec{H}_E^{A,B}$. The exchange field is $\vec{H}_E^{A,B} = \lambda\vec{M}^{B,A}$ with λ the exchange strength between two sublattice magnetizations [37]. The tensor is written as

$$\chi^{(iii)} = \chi^{(iiia)} + \chi^{(iiib)}, \tag{5}$$

with

$$\chi^{(iiia)} = \gamma M_0 \begin{pmatrix} \frac{(\gamma H_A - i\alpha\omega)}{\omega_r^2 - (\omega + \gamma H_0)^2} & i\frac{(\gamma H_A - i\alpha\omega)}{\omega_r^2 - (\omega + \gamma H_0)^2} \\ -i\frac{(\gamma H_A - i\alpha\omega)}{\omega_r^2 - (\omega + \gamma H_0)^2} & \frac{(\gamma H_A - i\alpha\omega)}{\omega_r^2 - (\omega + \gamma H_0)^2} \end{pmatrix} \tag{6}$$

and

$$\chi^{(iiib)} = \gamma M_0 \begin{pmatrix} \frac{(\gamma H_A - i\alpha\omega)}{\omega_r^2 - (\omega - \gamma H_0)^2} & -i\frac{(\gamma H_A - i\alpha\omega)}{\omega_r^2 - (\omega - \gamma H_0)^2} \\ i\frac{(\gamma H_A - i\alpha\omega)}{\omega_r^2 - (\omega - \gamma H_0)^2} & \frac{(\gamma H_A - i\alpha\omega)}{\omega_r^2 - (\omega - \gamma H_0)^2} \end{pmatrix}, \tag{7}$$

where the antiferromagnetic resonance frequency is $\omega_r = \gamma\sqrt{H_A^a(H_A^a + 2H_E^a)}$. For the sake of simplicity, the imaginary parts in the denominators of Eqs. (6) and (7) are not given.

With the Polder tensors, we first compare two cases in Fig. 1. From Eqs. (3) and (4), one can see that the two expressions of the tensors are almost the same, indicating that the magnon photon couplings in these two cases are of a similar mechanism. As discussed later, both couplings give rise to the anticrossing, i.e., level repulsion. However, two differences exist. First, the magnon frequency is different: One increases with H_0 while another decreases with H_0. Second, the off-diagonal elements in Eqs. (3) and (4) differ by a prefactor of -1. This arises from the fact that the magnetization precession in case (i) is right handed while in case (ii) it is left handed.

Further, an antiferromagnet has two magnon modes. As shown in Eqs. (6) and (7), one can see that the tensors of the modes with $\omega_r \pm \gamma H_0$ have similar structures to those in cases (i) and (ii). Therefore, the magnetization precessions proposed in cases (i) and (ii) are equivalent to two magnon modes of an antiferromagnet. The advantage of the antiparallel system in this work is the low frequency that can be implemented in a microwave cavity.

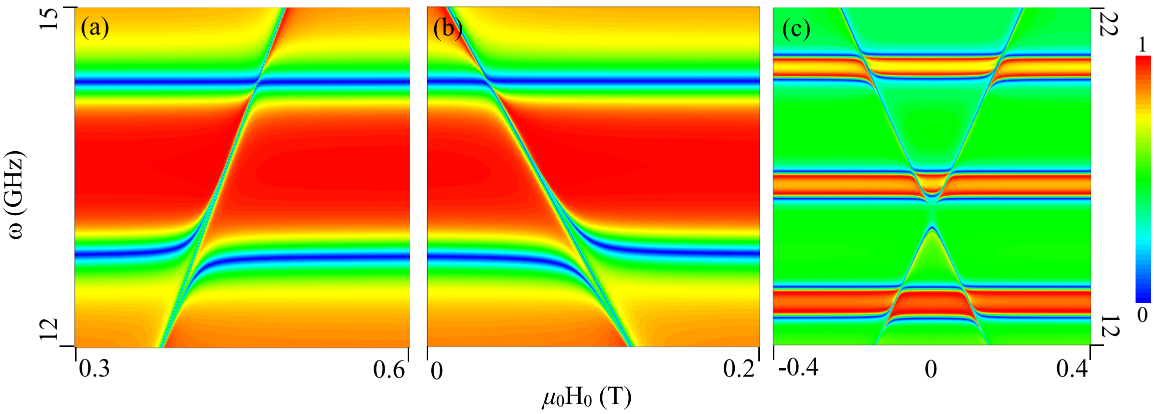

FIG. 2. $|S_{21}|$ spectrum of a ferromagnet-embedded cavity for (a) parallel alignment and (b) antiparallel alignment calculated with the method given in Sec. II. In each figure, the horizontal blue lines represent the odd mode (12.8 GHz) and even mode (14.3 GHz) of cavity resonance. The tilted lines represent the magnon mode and cross with cavity resonance to form level repulsion in (a) and (b). In the calculation of (b), we set a large anisotropic field of $H_A = 0.5$ T. (c) $|S_{21}|$ spectrum of an antiferromagnet-embedded cavity calculated with the method given in Ref. [37].

In order to demonstrate the magnon photon coupling, we consider a ferromagnet with parallel or antiparallel alignment inside a microwave cavity to calculate the transmission coefficient S_{21}. To do so, we introduce the Maxwell's equations

$$\nabla \times \vec{e} = -\frac{1}{c}\frac{\partial \vec{b}}{\partial t} = -\frac{\partial(\vec{h} + 4\pi\vec{m})}{\partial t}, \tag{8}$$

$$\nabla \times \vec{h} = \frac{1}{c}\frac{\partial(\epsilon_r \vec{e})}{\partial t}, \tag{9}$$

where $\vec{e}$, $\vec{b}$, $\vec{h}$, and $\vec{m}$ are the electric field, magnetic induction, magnetic field, and dynamic magnetization. ϵ_r and c are the relative permittivity and the speed of light in the vacuum.

By simultaneously solving the Maxwell's equations (8) and (9) and LLG equation (2), we can obtain the propagation state k inside the ferromagnet. With the propagation state, we can calculate the transfer matrix

$$\begin{pmatrix} e_y^d \\ h_x^d \end{pmatrix} = \begin{pmatrix} \cos(kd) & iZ\sin(kd) \\ i\frac{1}{Z}\sin(kd) & \cos(kd) \end{pmatrix} \begin{pmatrix} e_y^0 \\ h_x^0 \end{pmatrix}, \tag{10}$$

which connects the electric/magnetic fields at one surface ($z = 0$) and those at another surface ($z = d$) of a ferromagnet. $Z = \frac{\mu_s \omega}{k}$ is the impedance and the effective permeability μ_s is determined by $k = \frac{\omega}{c}\sqrt{\epsilon_r \mu_s}$. In this work, the relative permittivity ϵ_r is 15.0, the thickness d is 0.1 mm, and the Gilbert damping rate α is 1.25×10^{-4}. In the calculation of an antiferromagnet, the thickness d is 0.5 mm. The exchange and anisotropic fields are $H_E^a = 1.6$ T and $H_A^a = 0.1$ T.

Using the transfer matrix, we solve for the microwave transmission inside a microwave cavity that has been used in a recent experimental measurement [43]. The cavity is a circular waveguide with two circular-rectangular transitions at each end of the waveguide [43]. The length of the waveguide is 85.0 mm. To form a standing wave, a strong reflection of the intracavity wave is required. The reflection coefficient is 0.997 at the transitions. The phase change due to the reflection is 313.5°. More details of calculating the transmission coefficient can be found in Refs. [37,43]. As shown in Fig. 2, the S_{21} spectra of both parallel and antiparallel alignments present a level repulsion, but the mode polarization is opposite in Figs. 2(a) and 2(b). The antiferromagnetic magnon photon coupling in Fig. 2(c) shows an anticrossing gap of two magnons which could correspond to cases (i) or (ii).

III. TAVIS-CUMMINGS HAMILTONIAN

In the preceding section, we consider an explicit cavity geometry and material specifics to demonstrate magnon photon coupling of parallel and antiparallel alignments. In this section, we provide an intuitive discussion based on the Tavis-Cummings Hamiltonian. In the Tavis-Cummings model, the magnetization of a ferromagnet is represented by collective spin (magnon). The Hamiltonian is written as [44,45]

$$\begin{aligned} H = \hbar\omega_m S^z + \hbar\omega_c a^\dagger a + \hbar g_0(aS^+ + S^- a^\dagger) \\ + \hbar g_0(aS^- + S^+ a^\dagger), \end{aligned} \tag{11}$$

where $S^{x,y,z} = \Sigma_j s_j^{x,y,z}$ is the collective spin operator with s_j the operator of the jth spin. ω_m is the magnon frequency. The raising and lowering operators are $S^\pm = S^x \pm iS^y$. $a^\dagger$ (a) is the creation (annihilation) operator of photons with resonance frequency ω_c. g_0 is the coupling strength between a single spin and photon. The former two terms in the Hamiltonian are for a bare magnon and photon. The third and fourth terms describe the interaction between a magnon and photon.

In the case of parallel alignment shown in Fig. 1(a), the magnetization $\vec{M}$ is parallel to the effective magnetic field ($\vec{H}_{\text{eff}} = H_0\vec{z}$). Due to the relation $\vec{M} = -\gamma\vec{S}$, the spin angular momentum $\vec{S}$ is antiparallel to $\vec{H}_{\text{eff}}$ shown in Fig. 3(a). In the ground state, S^z takes the minimum value, i.e., $S^z = -S$ and thus $\omega_m = \omega_0 = \gamma H_0$. As a photon is absorbed, the spin angular momentum is deviated from the ground state ($S^z = -S$) and is promoted to the first excited state ($S^z = -S + 1$). In other words, a photon is annihilated while a magnon is created and vice versa. This is what the third term $(aS^+ + S^- a^\dagger)$ exactly refers to. Therefore, the fourth term does not matter, which is usually called the rotating wave approximation (RWA) [46].

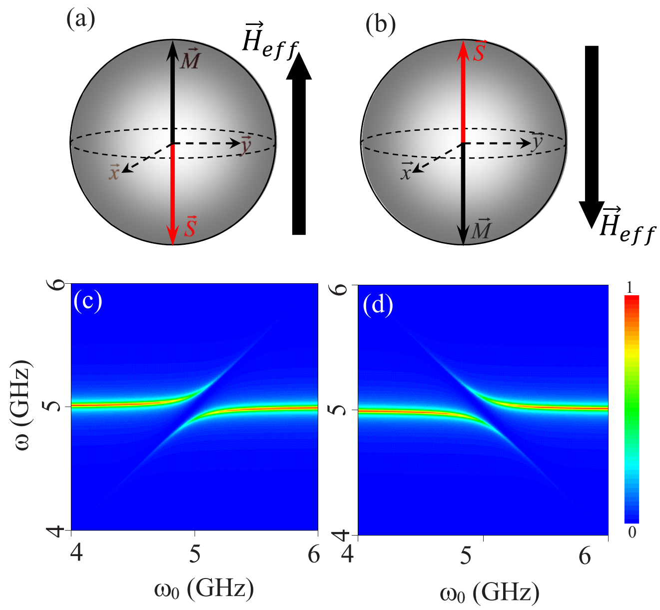

FIG. 3. Magnetization $\vec{M}$ and spin angular momentum $\vec{S}$ in the Bloch sphere representation. The static magnetic field $\vec{H}_0$ aligns along the $+\vec{z}$ direction while the effective magnetic field follows the magnetization. (a) $\vec{M} \parallel \vec{H}_0$ and $S^z = -S$ in the ground state; (b) $\vec{M} \parallel (-\vec{H}_0)$ and $S^z = +S$ in the ground state. (c) and (d) are the corresponding $|S_{21}|$ spectra of (a) and (b). The parameters used are $\omega_c = 5$ GHz, $g = 0.1$ GHz, and $\kappa_c = T_m = 0.01$ GHz.

As for antiparallel alignment in Fig. 1(b), the magnetization is antiparallel to the static magnetic field but follows the effective field [$\vec{H}_{\rm eff} = (H_0 - H_A)\vec{z}$]. In the ground state, S^z takes the maximum value, i.e., $S^z = +S$ and thus $\omega_m = \gamma(H_0 - H_A) = \omega_0 - \omega_A < 0$. The photon absorption results in a decrease of S^z from S to $S - 1$. Hence, only the fourth term in Eq. (11), i.e., $(aS^- + S^+a^\dagger)$, dominates.

We next calculate the transmission spectra based on the Tavis-Cummings Hamiltonian. In order to obtain quantum mechanical expectation values, we write the equation of motion for Eq. (11) and then add the dissipation terms into the equation. The resulting Bloch equation is written as

$$\frac{d}{dt}\begin{pmatrix}\langle a\rangle\\ \langle S^-\rangle\end{pmatrix} = \begin{pmatrix}-(\kappa_c + i\omega_c) & -ig_0\\ -i2g_0S & -(T_m + i\omega_m^{p,ap})\end{pmatrix}\begin{pmatrix}\langle a\rangle\\ \langle S^-\rangle\end{pmatrix}, \tag{12}$$

where $\omega_m^p = \omega_0$ and $\omega_m^{ap} = \omega_A - \omega_0$. κ_c and T_m are the damping rates of the photon and magnon. The above derivation is performed on the semiclassical limit with which the decoupling can be done, i.e., $\langle S^z a\rangle \propto \langle S^z\rangle\langle a\rangle$. Such a semiclassical limit implies that the quantum noise is excluded in our calculation which is valid in the experiment with large photon and magnon numbers. With this approximation, Eqs. (12) are close and thus can be solved analytically for the calculation of transmission. To do so, we consider the input-output theory [47] and introduce the microwave amplitudes propagating inwards the input port $a_{\rm in}$ and outwards the output port $a_{\rm out}$. Finally, the transmission coefficient is written as

$$S_{21} = \frac{\langle a_{\rm out}\rangle}{\langle a_{\rm in}\rangle} = \frac{\sqrt{\kappa_{\rm in}\kappa_{\rm out}}}{(\kappa_c + i\omega_c - i\omega) + \frac{2g_0^2S}{(T_m + i\omega_m^{p,ap} - i\omega)}}, \tag{13}$$

where $\kappa_{\rm in,out}$ is the coupling strength between the cavity and input (output) port. In the calculation of Eq. (13), the following parameters are chosen: $\omega_c = 5$ GHz, $g = 0.1$ GHz, $\kappa_c = T_m = 0.01$ GHz. The S_{21} spectrum is shown in Figs. 3(c) and 3(d), which is in good agreement with those shown in Fig. 2.

Furthermore, the Tavis-Cummings Hamiltonian, i.e., Eq. (11), can be transformed to a coupled Hamiltonian of two harmonic oscillators with the help of the Holstein-Primakoff (HP) transformation [37]. As for parallel alignment, the spin angular momentum starts from the lowest value (south pole) and increases to create a magnon. Hence, the HP transformation is written as

$$\begin{aligned} S^+ &= \sqrt{2S}b^\dagger,\\ S^- &= \sqrt{2S}b,\\ S^z &= -S + b^\dagger b, \end{aligned} \tag{14}$$

and Eq. (11) becomes

$$H^p = \hbar\omega_0 b^\dagger b + \hbar\omega_c a^\dagger a + \hbar\sqrt{2S}g_0(ab^\dagger + ba^\dagger). \tag{15}$$

As for antiparallel alignment, the spin angular momentum starts from the highest-energy position (north pole) and its decrease (increase) means the creation (annihilation) of a magnon. The HP transformation is thus written as

$$\begin{aligned} S^+ &= \sqrt{2S}b,\\ S^- &= \sqrt{2S}b^\dagger,\\ S^z &= S - b^\dagger b, \end{aligned} \tag{16}$$

and Eq. (11) becomes

$$H^{ap} = \hbar(\omega_A - \omega_0)b^\dagger b + \hbar\omega_c a^\dagger a + \hbar\sqrt{2S}g_0(ab^\dagger + ba^\dagger). \tag{17}$$

Equations (15) and (17) represent the coupling Hamiltonian of level repulsion, which has been widely used in the studies of a cavity magnon polariton [1–22].

IV. CONCLUSION

In summary, we investigate magnon photon coupling of a ferromagnetic system in which the magnetization is antiparallel with a static magnetic field. This system provides a magnon mode with a frequency that decreases with a static magnetic field. We analyzed the Polder susceptibility tensor and found that the tensors of parallel and antiparallel alignments have almost the same structure. This results in the level repulsion of magnon photon coupling for both alignments. In contrast to parallel alignment, the antiparallel alignment presents left-handed magnetization precession with respect to a static magnetic field and thus has a distinct magnon polarization. Further, one can find that the magnon modes of parallel and antiparallel alignments are analogous to two magnon modes of a antiferromagnet. In addition, we provide an intuitive analysis of magnon photon coupling based on the Tavis-Cummings Hamiltonian. It is shown that the photon absorption increases the spin angular momentum in parallel alignment while it decreases it in antiparallel alignment. The coupled Hamiltonians of two harmonic oscillators are also given. Due to the difficulty in the fabrication of a high-frequency cavity and low-damping material, the coupling between a photon and antiferromagnetic magnon is hard to observe. The system proposed in this paper provides an alternative method to study antiferromagnetic magnon photon coupling.

ACKNOWLEDGMENTS

This work is supported by the National Natural Science Foundation of China (NSFC61974067, 91750112, and 11804158). K.X. is supported by the National Natural Science Foundation of China (NSFC61774017, 11734004, and 12088101) and the NSAF (U1930402). We thank Professor Jiang Xiao for his helpful suggestions and comments.

[1] O. O. Soykal and M. E. Flatte, Phys. Rev. Lett. **104**, 077202 (2010).

[2] H. Y. Yuan, P. Yan, S. Zheng, Q. Y. He, K. Xia, and M. H. Yung, Phys. Rev. Lett. **124**, 053602 (2020).

[3] J. Graf, H. Pfeifer, F. Marquardt, and S. Viola Kusminskiy, Phys. Rev. B **98**, 241406(R) (2018).

[4] J. Li, S. Y. Zhu, and G. S. Agarwal, Phys. Rev. Lett. **121**, 203601 (2018).

[5] S. Sharma, Y. M. Blanter, and G. E. W. Bauer, Phys. Rev. B **96**, 094412 (2017).

[6] C. Braggio, G. Carugno, M. Guarise, A. Ortolan, and G. Ruoso, Phys. Rev. Lett. **118**, 107205 (2017).

[7] T. Liu, X. Zhang, H. X. Tang, and M. E. Flatte, Phys. Rev. B **94**, 060405(R) (2016).

[8] V. L. Grigoryan and K. Xia, Phys. Rev. B **99**, 224408 (2019).

[9] H. Huebl, C. W. Zollitsch, J. Lotze, F. Hocke, M. Greifenstein, A. Marx, R. Gross, and S. T. B. Goennenwein, Phys. Rev. Lett. **111**, 127003 (2013).

[10] Y. Tabuchi, S. Ishino, T. Ishikawa, R. Yamazaki, K. Usami, and Y. Nakamura, Phys. Rev. Lett. **113**, 083603 (2014).

[11] M. Goryachev, W. G. Farr, D. L. Creedon, Y. Fan, M. Kostylev, and M. E. Tobar, Phys. Rev. Appl. **2**, 054002 (2014).

[12] Y. P. Wang, G. Q. Zhang, D. Zhang, X. Q. Luo, W. Xiong, S. P. Wang, T. F. Li, C.-M. Hu, and J. Q. You, Phys. Rev. B **94**, 224410 (2016).

[13] N. J. Lambert, J. A. Haigh, and A. J. Ferguson, J. Appl. Phys. **117**, 053910 (2015).

[14] A. Osada, A. Gloppe, R. Hisatomi, A. Noguchi, R. Yamazaki, M. Nomura, Y. Nakamura, and K. Usami, Phys. Rev. Lett. **120**, 133602 (2018).

[15] Y. P. Wang, G. Q. Zhang, D. Zhang, T. F. Li, C. M. Hu, and J. Q. You, Phys. Rev. Lett. **120**, 057202 (2018).

[16] J. Bourhill, N. Kostylev, M. Goryachev, D. L. Creedon, and M. E. Tobar, Phys. Rev. B **93**, 144420 (2016).

[17] X. Zhang, N. Zhu, C. L. Zou, and H. X. Tang, Phys. Rev. Lett. **117**, 123605 (2016).

[18] A. Osada, R. Hisatomi, A. Noguchi, Y. Tabuchi, R. Yamazaki, K. Usami, M. Sadgrove, R. Yalla, M. Nomura, and Y. Nakamura, Phys. Rev. Lett. **116**, 223601 (2016).

[19] Y. Cao, P. Yan, H. Huebl, S. T. B. Goennenwein, and G. E. W. Bauer, Phys. Rev. B **91**, 094423 (2015).

[20] H. Maier-Flaig, M. Harder, R. Gross, H. Huebl, and S. T. B. Goennenwein, Phys. Rev. B **94**, 054433 (2016).

[21] L. Bai, M. Harder, P. Hyde, Z. Zhang, C. M. Hu, Y. P. Chen, and J. Q. Xiao, Phys. Rev. Lett. **118**, 217201 (2017).

[22] L. Bai, M. Harder, Y. P. Chen, X. Fan, J. Q. Xiao, and C. M. Hu, Phys. Rev. Lett. **114**, 227201 (2015).

[23] A. V. Sadovnikov, S. A. Odintsov, E. N. Beginin, S. E. Sheshukova, Yu. P. Sharaevskii, and S. A. Nikitov, Phys. Rev. B **96**, 144428 (2017).

[24] A. V. Sadovnikov, A. A. Grachev, S. E. Sheshukova, Yu. P. Sharaevskii, A. A. Serdobintsev, D. M. Mitin, and S. A. Nikitov, Phys. Rev. Lett. **120**, 257203 (2018).

[25] S. Haroche, Rev. Mod. Phys. **85**, 1083 (2013).

[26] G. Kurizki, P. Bertet, Y. Kubo, K. Molmer, D. Petrosyan, P. Rabl, and J. Schmiedmayer, Proc. Natl. Acad. Sci. USA **112**, 3866 (2015).

[27] A. Imamoglu, Phys. Rev. Lett. **102**, 083602 (2009).

[28] X. Zhang, C. L. Zou, L. Jiang, and H. X. Tang, Sci. Adv. **2**, e1501286 (2016).

[29] X. Zhang, C. L. Zou, N. Zhu, F. Marquardt, L. Jiang, and H. X. Tang, Nat. Commun. **6**, 8914 (2015).

[30] M. Harder and C. M. Hu, Solid State Phys. **69**, 47 (2018).

[31] B. M. Yao, Y. S. Gui, J. W. Rao, S. Kaur, X. S. Chen, W. Lu, Y. Xiao, H. Guo, K.-P. Marzlin, and C.-M. Hu, Nat. Commun. **8**, 1437 (2017).

[32] B. Zare Rameshti and G. E. W. Bauer, Phys. Rev. B **97**, 014419 (2018).

[33] X. Zhang, C. L. Zou, L. Jiang, and H. X. Tang, Phys. Rev. Lett. **113**, 156401 (2014).

[34] C. Match, M. Harder, L. Bai, P. Hyde, and C. M. Hu, Phys. Rev. B **99**, 134445 (2019).

[35] O. Johansen and A. Brataas, Phys. Rev. Lett. **121**, 087204 (2018).

[36] H. Y. Yuan and X. R. Wang, Appl. Phys. Lett. **110**, 082403 (2017).

[37] Y. Xiao, X. H. Yan, Y. Zhang, V. L. Grigoryan, C. M. Hu, H. Guo, and K. Xia, Phys. Rev. B **99**, 094407 (2019).

[38] J. R. Everts, G. G. G. King, N. J. Lambert, S. Kocsis, S. Rogge, and J. J. Longell, Phys. Rev. B **101**, 214414 (2020).

[39] M. Bialek, A. Magrez, and J.-Ph. Ansermet, Phys. Rev. B **101**, 024405 (2020).

[40] S. Mandal, L. N. Kapoor, S. Ghosh, J. Jesudasan, S. Manni, A. Thamizhavel, P. Raychaudhuri, V. Singh, and M. M. Deshmukh, Appl. Phys. Lett. **117**, 263101 (2020).

[41] V. Baltz, A. Manchon, M. Tsoi, T. Moriyama, T. Ono, and Y. Tserkovnyak, Rev. Mod. Phys. **90**, 015005 (2018).

[42] A. G. Gurevich and G. A. Melkov, *Magnetization Oscillations and Waves* (CRC Press, New York, 1996).

[43] B. M. Yao, Y. S. Gui, Y. Xiao, H. Guo, X. S. Chen, W. Lu, C. L. Chien, and C.-M. Hu, Phys. Rev. B **92**, 184407 (2015).

[44] R. H. Dicke, Phys. Rev. **93**, 99 (1954).

[45] M. Tavis and F. W. Cumming, Phys. Rev. **170**, 379 (1968).

[46] C. Cohen-Tannoudji, J. Dupont-Roc, and G. Grynberg, *Atom-Photon Interaction* (Wiley-VCH, Weinheim, 2004).

[47] A. A. Clerk, M. H. Devoret, S. M. Girvin, F. Marquardt, and R. J. Schoelkopf, Rev. Mod. Phys. **82**, 1155 (2010).